

GaussRender: Learning 3D Occupancy with Gaussian Rendering

Loick Chambon^{1,2}, Éloi Zablocki¹, Alexandre Boulch¹, Mickaël Chen³, Matthieu Cord^{1,2}

¹ Valeo.ai, Paris, France ² Sorbonne Université, Paris, France ³ Hcompany.ai, Paris, France.

Abstract

Understanding the 3D geometry and semantics of driving scenes is critical for developing of safe autonomous vehicles. While 3D occupancy models are typically trained using voxel-based supervision with standard losses (e.g., cross-entropy, Lovasz, dice), these approaches treat voxel predictions independently, neglecting their spatial relationships. In this paper, we propose GaussRender, a plug-and-play 3D-to-2D reprojection loss that enhances voxel-based supervision. Our method projects 3D voxel representations into arbitrary 2D perspectives and leverages Gaussian splatting as an efficient, differentiable rendering proxy of voxels, introducing spatial dependencies across projected elements. This approach improves semantic and geometric consistency, handles occlusions more efficiently, and requires no architectural modifications. Extensive experiments on multiple benchmarks (SurroundOcc-nuScenes, Occ3D-nuScenes, SSCBench-KITTI360) demonstrate consistent performance gains across various 3D occupancy models (TPVFormer, SurroundOcc, Symphonies), highlighting the robustness and versatility of our framework. The code is available at <https://github.com/valeoai/GaussRender>.

1. Introduction

Understanding the 3D geometry and semantics of driving scenes from a set of cameras is particularly challenging and crucial in autonomous driving. This has a direct impact on tasks such as object detection [29, 38, 41, 44, 49, 73, 95, 96], agent forecasting [12, 16, 34, 61, 63–65, 88], scene segmentation [3, 7, 17–20, 76] and is the main concern in 3D occupancy [24, 28, 39, 42, 75].

Existing methods for 3D scene understanding employ diverse representation spaces and input modalities, each with distinct advantages and limitations. Bird’s-eye view (BEV) representations [3, 7, 19, 41, 50, 79, 94] are popular as they integrate multi-sensor data well and are compatible with downstream tasks like planning [21, 81, 83] and forecasting [1, 19, 20, 90]. However, BEV representations collapse the height dimension, making them less effective at cap-

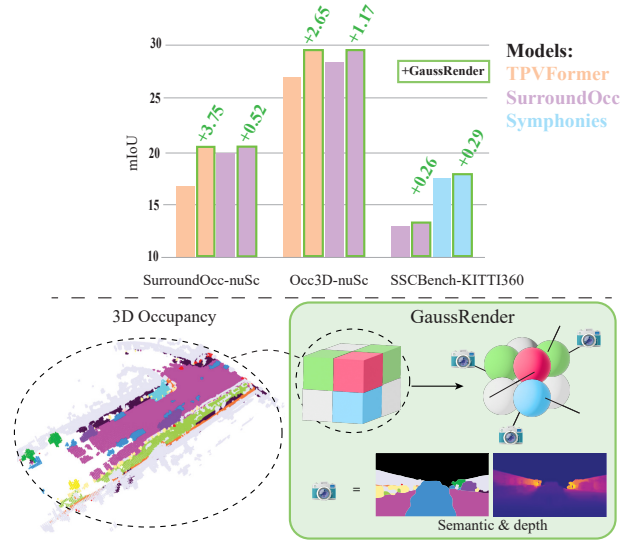


Figure 1. **GaussRender, a Voxel-to-Gaussian Based Rendering Module** consistently enhances the performance of 3D occupancy models across multiple datasets.

turing complex 3D geometries. Query-based methods provide task-specific and compact representations [44–46, 73], but their lack of interpretability poses challenges. In contrast, 3D-based representations preserve spatial details but are computationally expensive to train. In practice, methods using them are mostly trained with standard losses such as cross-entropy, dice [67], or Lovász [4], to supervise voxel predictions against ground truth. Nonetheless, these losses optimize predictions independently, neglecting the spatial relationships between voxels, as illustrated in Fig. 2. This limitation hinders the model’s ability to understand the entire geometry of an object, resulting in less effective training and geometrical understanding.

In this paper, we propose to address this limitation by integrating 3D-2D reprojection losses into the training of 3D occupancy models without modifying existing architectures and introducing only minimal computational overhead. The central idea is to project the predicted 3D voxel-based representation into 2D perspective views and supervise the model in the image space in addition to the standard 3D supervi-

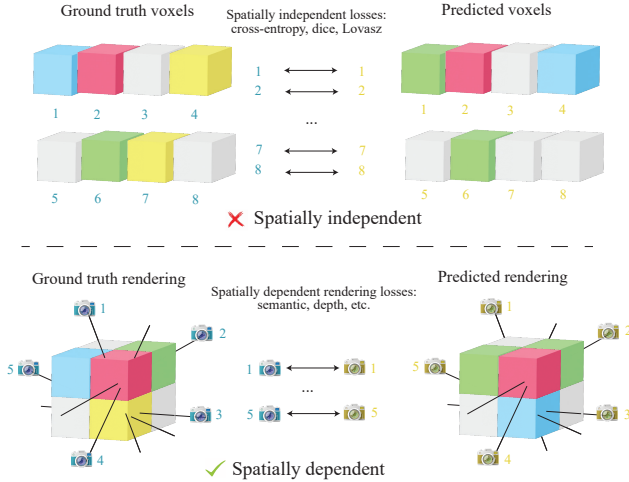


Figure 2. **Influence of Loss Functions on the Spatial Coherence of Voxels.** Standard 3D occupancy losses (top) are applied independently to each voxel, without enforcing spatial consistency as a voxel grid to be compared with voxel ground truths. In contrast, a rendering loss with GaussRender (bottom) promotes voxel consistency across the 3D space and enforces it from any viewpoint.

sions. To do so, our method, called GaussRender, creates a Gaussian proxy for each voxel before applying Gaussian splatting [9, 22, 32, 78, 87, 89] allowing to benefit from its lightweight and fast rendering without the overhead of traditional volume rendering techniques [2, 8, 54, 55]. By rendering 2D perspective projections, we introduce spatial relationships between elements projected on the same pixel, penalizing incoherent predictions and forcing the spatial semantic coherence of urban scenes. Moreover, our method can seamlessly leverage new viewpoints arbitrarily located in the scene, further improving occlusion handling and enriching supervision signals with diverse perspectives. By doing so, our approach consistently improves semantic and geometric understanding of all studied models on every studied dataset. The key contributions of our work include:

- A plug-and-play module computing semantic and depth rendering losses that improve 3D occupancy model’s training without requiring changes to existing architectures.
- The introduction of Gaussian splatting as an efficient proxy for voxel rendering in 3D occupancy tasks, reducing computational overhead.
- A viewpoint-agnostic supervision framework that leverages arbitrary camera poses for robust training.
- State-of-the-art results on three standard benchmarks, with significant gains in complex driving scenes.

2. Related work

2.1. Learning 3D semantic geometry from cameras

Many model representations exist in 3D occupancy tasks, all of which seek to be lightweight, redundancy-free, and capable of preserving the geometric and semantic understanding of the scene. These criteria are particularly important for 3D occupancy tasks, which require a high geometric and semantic understanding of the scene, and generally result in high memory costs due to the cubic representation of voxels. To overcome this, structured intermediate representation spaces such as tri-plane [24], octrees [51], tensor decompositions [92], BeV [36, 71], Gaussians [25, 27] or compact representations [52] have emerged alongside the development of the more traditional voxel-based representation in a multi-scale manner [75] with sometimes instance queries [28]. Regardless of the lifting procedure or intermediate representation, existing methods predict occupancy as a voxel grid to be compared with voxel ground truths. Thus, GaussRender is plugged once the final voxel grid is obtained. Our module computes an additional loss, making GaussRender architecture-agnostic.

Beyond feature representations, 3D occupancy models have focused on additional strategies to enhance performance. Aggregating past information refines scene representation, improves the understanding of occluded elements, and enhances current frame details [35, 36, 66, 84]. Some methods extend this to 4D forecasting, enabling spatio-temporal and semantic urban scene modeling [33, 52, 72, 80]. Self-supervised learning reduces dependency on voxel-based ground truths [14, 26] by estimating depth and semantic images from camera data. These methods compare learned representations against pseudo-labels. However, these pseudo-labels are often imprecise: depth estimation requires rescaling, and semantics may not align with dataset classes of 3D voxels. Supervised rendering utilizes ground truths from reprojected semantic lidar data [57]. While more precise than pseudo-annotations, lidar reprojections face challenges such as signal sparsity and occlusions. GaussRender agrees with the importance of using image projections for the 3D occupancy task, but we stress the importance of having both a dense representation as with self-supervision and an accurate representation as with lidar, without however requiring an external sensor. Whatever option is chosen for the ground truth, obtaining a comparable prediction invites us to discuss different ways of doing renderings.

2.2. Reprojecting 3D to 2D perspective views.

Adding voxel-based depth and semantic rendering losses requires projecting input and predicted voxels onto perspective image planes. While traditional differentiable rendering methods handle 3D modalities like point clouds and meshes

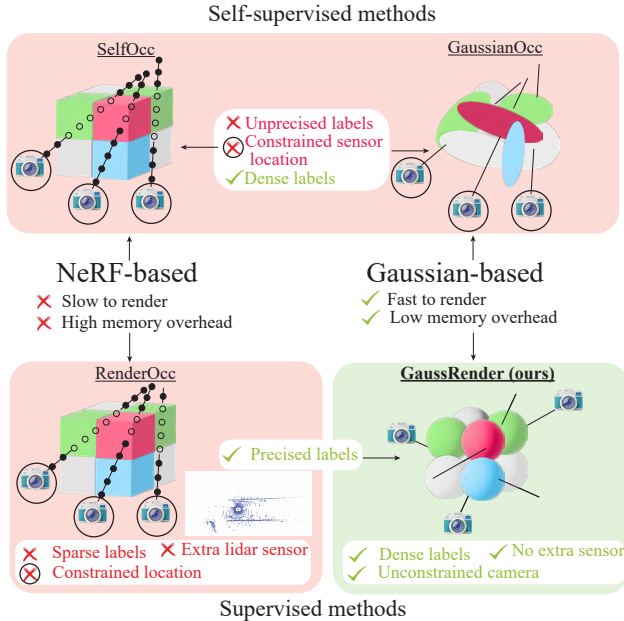


Figure 3. **Comparison of Rendering Methods on 3D Occupancy Predictions.** Previous methods rely on imprecise pseudo-annotations or require an additional lidar sensor, with losses computed in the sensor’s reference frame. In contrast, our approach GaussRender uses only voxel-based ground truths while allowing flexible rendering from any viewpoint.

[31, 47], recent approaches focus on neural rendering techniques and Gaussian-based methods to render other representations.

Previous 3D occupancy methods using lidar’s reprojections as input [26, 57] rely on NeRF-based techniques to render the predicted voxels. Neural Radiance Fields (NeRF) [2, 15, 30, 48, 53–55, 59, 86] encode spatial information as a continuous 5D function that maps 3D coordinates and viewing directions to color and density. A neural network predicts color and opacity at any point in space, allowing image synthesis through ray integration from the camera’s perspective. NeRF effectively captures fine details and complex light interactions, such as reflections and refractions. In practice, such 3D occupancy methods using NeRF rely on point sampling along rays. This has the drawback that higher sampling frequencies or high-resolution renderings increase memory usage. In addition, this rendering is also sensitive to image quality and occlusions, which has led to the development of auxiliary ray techniques [57, 68] to overcome occlusions. GaussRender does not use such techniques and we based our module on another rendering technique.

Recently, a Gaussian reprojection technique has emerged [32]. It allows any 3D Gaussian to be reprojected onto a 2D Gaussian on an image while giving a close shape to the

Gaussian parameters and taking into account the accumulation of Gaussians per pixel. This has enabled even more realistic rendering, with a lower memory footprint. Initially used for scene rendering, it has been extended to a wide range of tasks, from scene editing [10, 74, 82] to physical rendering [13, 58, 62, 77] and generation [11, 60, 69, 85]. Gaussian representations have recently been used in many autonomous driving-related tasks: in pre-training [14], world models [97], as representations for end-to-end tasks [93], and as a 3D occupancy representation [25, 27]. In self-supervision, GaussianOcc [14] uses a similar rendering approach but has pseudo-labels as ground truth. In addition to having annotations that are estimated and therefore of lesser quality than the ground truth, their reprojections are only possible in existing cameras because they need RGB images to estimate their pseudo-labels. GaussRender allows rendering from any viewpoint with precise annotations. To our knowledge, our approach is the first to study the impact of a Gaussian rendering loss based solely on voxel annotations regardless of the model feature representation. A recently published concurrent work [68] proposes a Gaussian rendering loss but their study is limited to a single model and derives the ground truth using an additional modality, the lidar. Since the lidar signal suffers from the previously mentioned drawbacks, mainly occlusion and sparsity, they developed auxiliary ray techniques based on adjacent frames. In our case, thanks to perfect alignment, such tricks are unnecessary and we are able to compute our loss from any viewpoint.

3. GaussRender

We present GaussRender, a plug-and-play rendering method to enhance 3D occupancy models. First, we explain how to plug our module within standard pipelines (Sec. 3.1), then we detail our Gaussian rendering approach (Sec. 3.2), and finally, we explain multi-view supervision from arbitrary cameras (Sec. 3.3).

3.1. Integration of GaussRender in 3D occupancy pipelines

Classically, vision-to-3D semantic occupancy models take a set of N images $I = \{I_i\}_{i=1}^N$ and predict a 3D semantic grid of the scene $O \in C^{X \times Y \times Z}$, where C is the number of semantic classes considered, and (X, Y, Z) represents the spatial resolution of the scene.

The standard pipeline has three steps. (1) *Feature extraction*: Images pass through a backbone network to produce 2D features $F = \{F_i\}_{i=1}^N \in \mathbb{R}_{img}^d$, where d_{img} is the number of channels for each image. (2) *3D lifting*: Features are projected into 3D representations (e.g., voxels, tri-planes, etc.) using cross-attention and self-attention blocks. (3) *Voxel prediction*: All representations convert to voxels for loss computation against ground truth, using a combination of

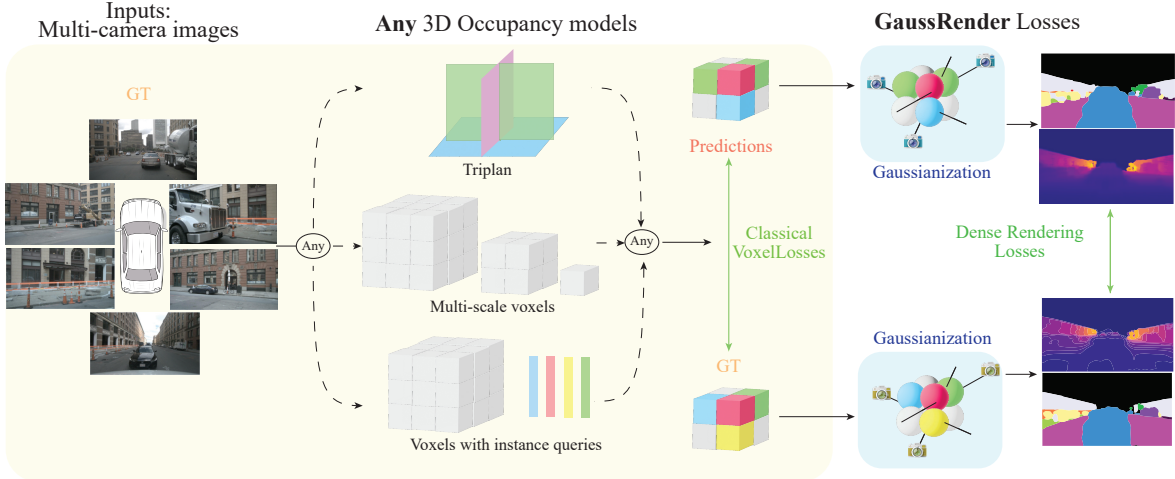


Figure 4. **Overview of GaussRender.** Unlike previous approaches, our rendering operates solely on 3D voxel data, without relying on point clouds. This eliminates issues related to sparse signals and occlusions. Additionally, Gaussian rendering avoids the sampling challenges of NeRF-based methods and benefits from the faster computation of Gaussian splatting [32].

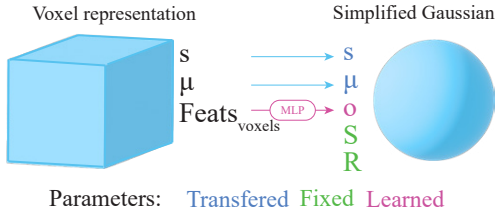


Figure 5. **Gaussianization of Voxels.** Each voxel (left) is converted to a 3D simplified Gaussian (right) with fixed position μ , scale S , and learned opacity o . Semantics s are inherited directly from the voxel predictions. The rotation R is set to the identity matrix (no orientation of Gaussians).

geometric and voxellic losses.

Our method operates at the final stage, as shown in Fig. 4, making it compatible with any 3D occupancy architecture.

3.2. Gaussian Rendering

As the core idea is to project 3D semantic voxel representation into 2D perspective views, we aim at rendering 3D voxels in an efficient and differentiable way. We thus build a rendering strategy with Gaussian Splatting [32], which enables faster rendering than traditional ray-casting approaches while maintaining differentiability for gradient backpropagation.

As illustrated in Fig. 5, we intentionally simplify the Gaussian parametrization of voxels to simple spheres, to avoid degenerate configurations from unconstrained optimization (fixed position, scale, and rotation), and preserve the model’s original class confidence scores (transfer of the semantics). For each voxel at position $\mu = (x, y, z)$, we

thus create a simple Gaussian primitive with:

- μ : position inherited from voxel grid coordinates.
- s : semantic class from the model’s final prediction.
- o : opacity learned from voxel features, when such features exist in the default model, or from the logit of the empty semantic class.
- $S = (s_x, s_y, s_z)$: fixed scale determined from voxel dimensions.
- $R = I$: rotation equals to identity (no orientation).

Then, the equations related to Gaussians remain unchanged, so the Gaussian covariance matrix Σ and the rendering giving to each pixel a ‘color’ C corresponding to the rendered semantic of the Gaussians, are computed as follows:

$$\Sigma = RSS^T R^T \quad \text{and} \quad C = \sum_{i=1}^N T_i \alpha_i \mathbf{c}_i$$

$$\text{with } \alpha_i = \left(1 - \exp(-\sigma_i \delta_i)\right) \text{ and } T_i = \prod_{j=1}^{i-1} (1 - \alpha_j)$$

where i indexes the Gaussians projected on the considered pixel, σ represent the density and δ the distance along the ray.

For ground-truth generation, we follow the same procedure but we render only the occupied voxels, assigning them an opacity of 1. Otherwise, we use the same scale for rendering the predictions, and we always position the Gaussians at the voxel locations.

Overall, this differentiable rendering enables supervision through 2D reprojection losses maintaining spatial relationships between voxels — a critical feature missing in traditional voxel-wise losses.

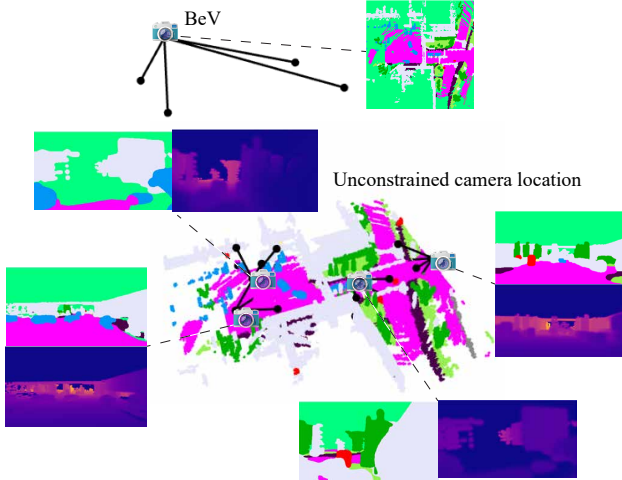


Figure 6. **Arbitrary Camera Positioning** in the scene with corresponding RGB and depth renderings. Virtual cameras can be placed freely to enhance voxel consistency by providing complementary information from diverse viewpoints, unlike previous methods restricted to the sensor’s original perspectives.

3.3. 2D ground truth from arbitrary cameras

Camera placement strategy. Our module can render views from any camera position in the scene, unlike previous approaches that are limited to the sensor’s original and fixed perspective. This flexibility allows for the supervision of the learning process from several different angles, including areas that are not visible to the original sensors. We achieve this by modifying the camera parameters: both the intrinsic and the extrinsic parameters, i.e., the type and the location of the cameras, as illustrated in Fig. 6.

A judicious choice of camera location depends on the complexity of the task. Depending on whether we prioritize only visible voxels or also aim to complete invisible voxels, we adopt a different strategy. In the latter case, we position the cameras to capture voxels that are invisible from the sensor, thereby providing a more external supervision signal. The adopted strategy is to elevate the cameras and tilt them slightly so they can see beyond the sensor while still sharing a significant amount of information. For more details on camera positioning, see Sec. 4.

Nevertheless, given the importance of the Bird’s Eye View (BeV) understanding in autonomous driving tasks, we systematically add a virtual BeV camera to obtain a more accurate representation. This also helps provide additional information about voxels that are not visible from the sensors.

2D-rendering loss. Each rendering produces both a semantic and a depth image. We compute respective L1 losses based on these renderings:

$$L_{\text{depth}}^{\text{cam}} = \left| \text{Depth}_{\text{pred}}^{\text{cam}} - \text{Depth}_{\text{gt}}^{\text{cam}} \right|$$

$$L_{\text{semantic}}^{\text{cam}} = \left| \text{Sem}_{\text{pred}}^{\text{cam}} - \text{Sem}_{\text{gt}}^{\text{cam}} \right|$$

where $\text{Depth}^{\text{cam}}$ stands for the rendered depth images on an arbitrary camera, Sem^{cam} stands for the semantic renderings on an arbitrary camera and ”pred” denotes images derived from predicted voxels while ”gt” denotes image derived from ground truths.

Concerning BeV rendering (marked with a ^{bev} tag), since it is positioned far from the scene, we only compute a semantic loss (removing the depth loss):

$$L_{\text{semantic}}^{\text{bev}} = \left| \text{Sem}_{\text{pred}}^{\text{bev}} - \text{Sem}_{\text{gt}}^{\text{bev}} \right|$$

Thus, the overall 2D rendering loss for our module is defined as:

$$L_{2\text{D}} = \frac{1}{N_{\text{cam}}} \sum_{\text{cam}} L_{\text{depth}}^{\text{cam}} + \frac{1}{N_{\text{cam}}} \sum_{\text{cam}} L_{\text{semantic}}^{\text{cam}} + L_{\text{semantic}}^{\text{bev}}$$

Training loss. Finally, the training loss of the model is simply the sum of the original 3D training losses $L_{3\text{D}}$ as a combination of cross-entropy, Lovasz and dice losses and our 2D rendering loss:

$$L = L_{3\text{D}} + \lambda L_{2\text{D}}$$

where λ is the weighting factor of the 2D loss. It is equal to 5 in all our experiments to have a contribution roughly equal to that of 3D loss.

4. Experiments

In this section, we evaluate GaussRender on several models and datasets to demonstrate the versatility of our rendering module. We present experimental details in Sec. 4.1, compare our results against state-of-the-art models and datasets in Sec. 4.2, show how GaussRender enhances 3D semantic occupancy predictions from multiple views in Sec. 4.3, and present some ablations of our method in Sec. 4.4.

4.1. Data and models

Data. The training and evaluation are conducted on three datasets: SurroundOcc-nuScenes [75], Occ3d-nuScenes [70], and SSCBench-Kitti360 [40].

SurroundOcc-nuScenes is derived from the nuScenes dataset [5], acquired in Boston and Singapore. It aggregates the lidar annotations of nuScenes to create 3D semantic occupancy grids of 50cm³ resolution, with labels corresponding to 17 lidar semantic segmentation classes. This dataset

takes into account both visible and occluded voxels. The occluded voxels are obtained by accumulating lidar data over the frames of the whole sequence consequently introducing temporal artefacts over dynamic objects.

Occ3D-nuScenes is also based on nuScenes dataset. It contains 18 semantic classes and has a voxel grid of 40cm^3 resolution. One major difference with SurroundOcc-nuScenes, is that Occ3D only evaluates the voxels visible from the cameras at the current time frame. It does not have lidar accumulation. Thus, it focuses on the geometric and semantic understanding of the visible objects, rather than extrapolating to occluded regions, leading to a simpler task.

SSCBench-Kitti360 [40] is derived from the Kitti360 dataset [43], acquired in Germany. It contains 19 semantic classes and has a voxel grid of 20cm^3 resolution resulting in a very precise semantic of the urban scenes. It takes into account during evaluation both visible and occluded voxels.

We briefly outline above the specific characteristics of each dataset regarding the 3D occupancy task, but more details can be found in App. A.

Models and training details. We plug GaussRender into three different models using different intermediate representations: **SurroundOcc** [75] (multi-scale voxel-based approach), **TPVFormer** [24] (tri-plane-based approach), and **Symphonies** [28] (voxel-with-instance query-based approach). By doing so we validate the claim that our proposed approach is compatible with any type of architecture. For each combination of models and datasets, we follow the same procedure. By default, if provided, we evaluate author checkpoints; if not, we report scores from previous papers; otherwise, we re-trained the models for the target dataset. Each trained model uses the same training settings, following the optimization parameters of [75]. More training details can be found in App. B.

4.2. GaussRender leads to state-of-the-art results.

4.2.1. 3D semantic occupancy results

We evaluate GaussRender across multiple models and datasets for 3D semantic occupancy prediction. Our method consistently improves performance without requiring other sensors such as the lidar used in certain methods [57, 68]. Results are summarized in Tab. 1 and detailed scores by class can be found in Appendix E.

SurroundOcc-nuScenes. On the SurroundOcc-nuScenes dataset [75] (considering visible and occluded voxels), GaussRender brings significant gains to all tested models. As shown in Tab. 1, TPVFormer [24] and SurroundOcc [75] reach the top two ranks. They achieve higher IoU (+1.2% and +1.1%) and mIoU (+3.8% and +0.5%) compared to their original implementations. Remarkably, GaussRender enables these models to surpass recent approaches like GaussianFormerV2 [25] in both IoU and

Model	Surround-Occ nusc. val.		Occ3D nusc. val.	SSCBench KITT360 test.	
	IoU	mIoU	mIoU	IoU	mIoU
BEVDet [23]	-	-	19.38	-	-
BEVStereo [37]	-	-	24.51	-	-
RenderOcc (L) [57]	-	-	23.93	-	-
RenderOcc (V+L)[57]	-	-	26.11	-	-
CTF-Occ [70]	-	-	28.53	-	-
TPVFormer-lidar [24]	11.51	11.66	-	-	-
MonoScene [6]	23.96	7.31	6.06	37.87	12.31
Atlas [56]	28.66	15.00	-	-	-
GaussianFormer [27]	29.83	19.10	-	-	-
BEVFormer [41]	30.50	16.75	26.88	-	-
GaussianFormerv2 [25]	30.56	20.02	-	-	-
VoxFormer [39]	-	-	-	38.76	11.91
OccFormer [91]	31.39	19.03	21.93	40.27	13.81
TPVFormer [24]	30.86	17.10	27.83	-	-
w/ GaussRender	32.05	20.85	30.48	-	-
	+1.19	+3.75	+2.65	-	-
SurroundOcc [75]	31.49	20.30	29.21	38.51	13.08
w/ GaussRender	32.61	20.82	30.38	38.62	13.34
	+1.12	+0.52	+1.17	+0.11	+0.26
Symphonies [†] [28]	-	-	-	43.40	17.82
w/ GaussRender	-	-	-	44.08	18.11
	-	-	-	+0.68	+0.29

Table 1. **Performance Comparison on Multiple 3D Occupancy Benchmarks.** We report IoU and mIoU metrics on SurroundOcc-nuScenes [75], Occ3D-nuScenes [70], and SSCBench-KITT360 [40]. The best results are highlighted in bold. Our module, GaussRender, consistently improves performance when integrated with standard models, achieving state-of-the-art results across all benchmarks. Performance gains introduced by GaussRender are shown in green.

mIoU, proving that older architectures can achieve state-of-the-art results when we plug GaussRender.

Occ3D-nuScenes. On Occ3D-nuScenes [70] (filtering unobserved voxels), GaussRender produces the top two results: TPVFormer with GaussRender achieves 30.48 mIoU (+2.65), ranking first, and SurroundOcc with GaussRender reaches 30.38 mIoU (+1.17), ranking second. Notably, our approach outperforms RenderOcc [57] without requiring lidar inputs for loss computation. This demonstrates GaussRender’s ability to learn effective 3D representations using only cameras.

SSCBench-Kitti360. On the challenging SSCBench-Kitti360 [43] dataset we observe +0.26 mIoU / +0.11 IoU gains for SurroundOcc [75] and +0.29 mIoU / +0.68 IoU gains for Symphonies [28]. While absolute gains appear smaller here, models in this benchmark achieve tightly clustered performance due to the smaller voxel size making the

Dataset	Model	BeV		Image		Depth
		IoU ^{BeV} (\uparrow)	mIoU ^{BeV} (\uparrow)	IoU ^{Img} (\uparrow)	mIoU ^{Img} (\uparrow)	L1 ^{Img} (\downarrow)
SurroundOcc-nuSc [75]	TPVFormer [24]	58.16	28.48	88.63	52.93	1.96
	w/ GaussRender	59.08 +0.82	28.51 +0.03	90.79 +2.16	52.97 +0.04	1.78 -0.18
	SurroundOcc [75]	58.49	27.92	88.02	48.25	2.04
	w/ GaussRender	60.37 +1.88	28.43 +0.51	91.35 +3.32	49.06 +0.81	1.77 -0.27
Occ3D-nuSc [70]	TPVFormer [24]	52.99	29.15	82.92	54.73	2.40
	w/ GaussRender	54.36 +1.37	29.64 +0.49	89.66 +6.68	58.07 +3.34	1.93 -0.47
	SurroundOcc [75]	53.62	28.45	83.63	51.02	2.38
	w/ GaussRender	55.51 +1.89	29.87 +1.42	90.00 +6.37	56.54 +5.52	1.85 -0.53

Table 2. **Impact of GaussRender on Image, Depth, and BeV metrics.** Comparison of BeV (IoU^{BeV}, mIoU^{BeV}), image-based (IoU^{Img}, mIoU^{Img}), and depth metrics (L1^{Img}) across datasets. Best results per dataset/metric are bolded with green performance deltas.

Supervision	2D ground-truth	IoU (\uparrow)	mIoU (\uparrow)
SelfOcc [26]	Pseudo-labels	-	9.30
GaussianOcc [14]	Pseudo-labels	-	9.94
RenderOcc [57]	Lidar	-	19.33
GSRender [68]	Lidar	-	21.36
GaussRender	Voxels	41.14	22.15 +0.79

Table 3. **Performance Comparison of Models trained with 2D Ground Truth on Occ3d-nuScenes validation set.** We used a TPVFormer model to train 3D occupancy with L_{2D} loss without L_{3D} loss. Previous results are reported from [68]. ‘Pseudo-labels’ refer to 2D annotations generated via depth and semantic estimation models, ‘Lidar’ denotes labels obtained through lidar-to-image reprojection, and ‘Voxels’ correspond to Gaussian rendering performed on voxel representations. The best results are in bold.

segmentation task more difficult. — even modest improvements are difficult to achieve.

Our results show that GaussRender consistently enhances various architectures leading to state-of-the-art results, reaches top results without requiring projected lidar annotations, and remains effective across different dataset scales and annotation densities. This demonstrates the fundamental benefits of GaussRender for 3D semantic occupancy learning.

4.2.2. Training with only 2D rendering objective

To evaluate the effectiveness of GaussRender to capture the semantics and the geometry of urban scenes. We isolate our module by comparing the 3D IoU and mIoU of a class of models doing 3D occupancy solely trained with 2D supervision (L_{2D}) without 3D supervision (L_{3D}). To compare with other methods, we plug GaussRender into TPVFormer. As shown in Tab. 3, with 22.15 mIoU, it outperforms both RenderOcc [57] (+2.82 mIoU) and GSRender [68] (+0.79 mIoU). Moreover, unlike these methods, GaussRender does not require auxiliary rays from adjacent frames, making it simpler to implement and computationally less expensive.

4.3. Finer-grained multi-view metric analysis

Classical 3D semantic occupancy metrics provide aggregated scene-level scores, treating all voxels with equal importance. This can dilute performance variations across regions, and viewpoints, and does not fully reflect the model’s ability to localize objects and surfaces accurately — one of the key objectives of the 3D semantic occupancy task. To address this, we introduce in the context of 3D occupancy training, additional evaluation metrics that capture different aspects of spatial understanding. Bird’s-Eye-View (BeV) metrics — critical for motion forecasting and planning — measure spatial accuracy using IoU^{BeV} and mIoU^{BeV}. In parallel, sensor-view metrics assess geometric and semantic consistency from the perspective of the original ego-vehicle position through IoU^{Img}, mIoU^{Img}, and L1^{Img} depth error.

To ensure a fair comparison and quantify the potential gains provided by our module, we convert voxel outputs of models trained with and without GaussRender to Gaussian representations using a unified protocol. Voxels are converted to Gaussian using fixed scales aligned with ground truth, semantic labels transferred from voxel predictions, and an opacity set to 1 for occupied voxels. Then, the renderings are calculated.

Our multi-view analysis is presented in Table 2. We observe that the use of GaussRender enhances all metrics simultaneously, with systematic gains associated with different combinations of datasets and models. We particularly note gains in image-space IoU of +2.16 / +6.68 and in depth L1 error of -0.18 / -0.53. But also GaussRender improves spatial understanding with BEV IoU gains of +0.82 / +1.89. Moreover, both TPVFormer and SurroundOcc show significant improvements across all datasets and evaluations. This evaluation highlights that the use of GaussRender not only improves 3D occupancy predictions but also enhances consistency with BeV and 2D sensor observations.

Camera positioning	SurroundOcc-nuSc [75]		Occ3d-nuSc [70]	
	IoU (\uparrow)	mIoU (\uparrow)	IoU (\uparrow)	mIoU (\uparrow)
Sensor	27.3	10.7	41.14	22.15
Elevated	28.4	11.2	40.0	15.2
Random	28.0	9.3	40.1	12.7

Table 4. **Impact of different Camera Positioning Strategies on 3D semantic occupancy performances.** The architecture used is TPVFormer [24]. Models are trained using only L_{2D} without L_{3D} but are evaluated on 3D IoU and mIoU.

4.4. Ablations studies

4.4.1. Impact of supervising with virtual viewpoints

A key advantage of GaussRender is that instead of relying on lidar data and specific ray configurations we directly render voxels allowing us to render from arbitrary viewpoints. To explore the impact of different virtual camera placements, we evaluate several positioning strategies described below:

- **Sensor Strategy:** Cameras are placed at the original positions and orientations from the dataset.
- **Random Strategy:** Cameras are randomly positioned within the scene by applying a pitch and yaw variation of $\pm 10^\circ$ and a forward-backward shift from $\pm 10m$ relative to the original ego position.
- **Elevated Strategy:** Cameras are lifted by 8m while tilted 20° downward. This provides a wider field of view and reduces voxel occlusion.

Table 4 quantifies the impact of these strategies on the final 3D predictions. The choice of camera placement should be tailored to the specific task. If the goal is to predict only visible voxels, as in Occ3D-nuScenes [70], using sensor-aligned viewpoints yields the best results. However, if the objective is to also infer occluded regions, as in SurroundOcc-nuScenes [75], placing virtual cameras to maximize the visibility of these areas provides better supervision. The random strategy further highlights the importance of careful camera positioning: placing cameras arbitrarily often leads to poor 3D metrics, as they mainly observe empty space.

4.4.2. Gaussianization of voxels

An important parameter of our rendering process is the fixed size of the Gaussians used to represent voxels. To study the impact of the Gaussian scale, we train a TPVFormer [24] model on Occ3d-nuScenes [70], and vary the scale for both ground-truth and predicted renderings. In this study, we trained models using only the 2D rendering losses (Sec. 3.3), omitting the usual 3D voxel losses to focus on the effect of scale on rendering metrics.

Our results, in Fig. 7, indicate that the Gaussian scale

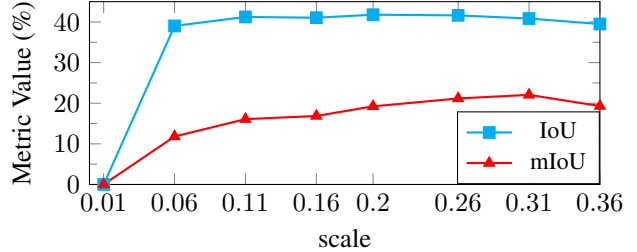


Figure 7. **Impact of Fixed Gaussian Scales on 3D mIoU and IoU** using TPVFormer [24] trained using only L_{2D} without L_{3D} on Occ3d-nuScenes [70] validation set.

is critical to the model’s performance. We need to find the right balance: if the Gaussians are too large, only a few will cover the entire image and the loss will be backpropagated mainly from the closest elements. Conversely, if the Gaussians are too small, gaps will appear between the voxels, resulting in a sparse activation that causes the model to render only the empty class, yielding very low metric values.

From a theoretical point of view, since voxels have a fixed size, it is logical that the optimum size should be related to the size of the voxels. The intuition is to represent a voxel by a spherical Gaussian with a standard deviation such that $2\sigma = c$ where c is the voxel side, i.e., analytically, for Occ3d-nuScenes and SurroundOcc-nuScenes we obtain $\sigma = 0.25$ and for SSCBench-KITTI360, $\sigma = 0.1$.

5. Conclusion

In this paper, we propose GaussRender a Gaussian rendering module tailored for 3D occupancy tasks. Our Gaussian-based rendering requires no external sensor and operates solely on voxels, making it compatible with any existing architecture and achieving performance improvements across all studied datasets and models leading to state-of-the-art results.

GaussRender is easy to plug and introduces only a single degree of freedom (the scale of the Gaussians) while maintaining a low computational and memory overhead and allowing to render voxels from any viewpoint. In addition, we show that systematically using loss functions that enhance the spatial coherence of 3D predictions is essential to improve 3D occupancy results while ameliorating 3D-2D consistency between voxels and their reprojection in the image and in BeV.

Acknowledgments

This work was partially supported by the ANR MultiTrans project (ANR-21-CE23-0032). This work was granted access to the HPC resources of IDRIS under the allocation AD011014252R1 made by GENCI.

References

- [1] Adil Kaan Akan and Fatma Güney. Stretchbev: Stretching future instance prediction spatially and temporally. In *Computer Vision - ECCV 2022 - 17th European Conference, Tel Aviv, Israel, October 23-27, 2022, Proceedings, Part XXXVIII*, 2022. 1
- [2] Jonathan T. Barron, Ben Mildenhall, Matthew Tancik, Peter Hedman, Ricardo Martin-Brualla, and Pratul P. Srinivasan. Mip-nerf: A multiscale representation for anti-aliasing neural radiance fields, 2021. 2, 3
- [3] Florent Bartoccioni, Eloi Zablocki, Andrei Bursuc, Patrick Pérez, Matthieu Cord, and Karteek Alahari. Lara: Latents and rays for multi-camera bird’s-eye-view semantic segmentation. In *Conference on Robot Learning, CoRL 2022, 14-18 December 2022, Auckland, New Zealand, 2022*. 1
- [4] Maxim Berman, Amal Rannen Triki, and Matthew B Blaschko. The lovász-softmax loss: A tractable surrogate for the optimization of the intersection-over-union measure in neural networks. In *Proceedings of the IEEE Conference on Computer Vision and Pattern Recognition*, pages 4413–4421, 2018. 1
- [5] Holger Caesar, Varun Bankiti, Alex H. Lang, Sourabh Vora, Venice Erin Liong, Qiang Xu, Anush Krishnan, Yu Pan, Giancarlo Baldan, and Oscar Beijbom. nuscenes: A multi-modal dataset for autonomous driving. In *2020 IEEE/CVF Conference on Computer Vision and Pattern Recognition, CVPR 2020, Seattle, WA, USA, June 13-19, 2020*, 2020. 5, 1
- [6] Anh-Quan Cao and Raoul de Charette. Monoscene: Monocular 3d semantic scene completion. In *CVPR, 2022*. 6, 3
- [7] Loïck Chambon, Éloi Zablocki, Mickaël Chen, Florent Bartoccioni, Patrick Pérez, and Matthieu Cord. Pointbev: A sparse approach to bev predictions. In *IEEE/CVF Conference on Computer Vision and Pattern Recognition, CVPR 2024, Seattle, WA, USA, June 16-22, 2024*, 2024. 1
- [8] Anpei Chen, Zexiang Xu, Andreas Geiger, Jingyi Yu, and Hao Su. Tensorf: Tensorial radiance fields. *arXiv preprint arXiv:2203.09517*, 2022. 2
- [9] Anpei Chen, Haofei Xu, Stefano Esposito, Siyu Tang, and Andreas Geiger. Lara: Efficient large-baseline radiance fields. In *Computer Vision - ECCV 2024 - 18th European Conference, Milan, Italy, September 29-October 4, 2024, Proceedings, Part XI*, 2024. 2
- [10] Yiwen Chen, Zilong Chen, Chi Zhang, Feng Wang, Xiaofeng Yang, Yikai Wang, Zhongang Cai, Lei Yang, Huaping Liu, and Guosheng Lin. Gaussianeditor: Swift and controllable 3d editing with gaussian splatting. In *IEEE/CVF Conference on Computer Vision and Pattern Recognition, CVPR 2024, Seattle, WA, USA, June 16-22, 2024*, 2024. 3
- [11] Jaeyoung Chung, Suyoung Lee, Hyeongjin Nam, Jaerin Lee, and Kyoung Mu Lee. Luciddreamer: Domain-free generation of 3d gaussian splatting scenes. *CoRR*, 2023. 3
- [12] Lan Feng, Mohammadhossein Bahari, Kaouther Mersaoud Ben Amor, Éloi Zablocki, Matthieu Cord, and Alexandre Alahi. Unitraj: A unified framework for scalable vehicle trajectory prediction. *arXiv preprint arXiv:2403.15098*, 2024. 1
- [13] Yutao Feng, Xiang Feng, Yintong Shang, Ying Jiang, Chang Yu, Zeshun Zong, Tianjia Shao, Hongzhi Wu, Kun Zhou, Chenfanfu Jiang, and Yin Yang. Gaussian splashing: Unified particles for versatile motion synthesis and rendering. *arXiv preprint arXiv:2401.15318*, 2024. 3
- [14] Wanshui Gan, Fang Liu, Hongbin Xu, Ningkai Mo, and Naoto Yokoya. Gaussianocc: Fully self-supervised and efficient 3d occupancy estimation with gaussian splatting. *CoRR*, 2024. 2, 3, 7
- [15] Stephan J. Garbin, Marek Kowalski, Matthew Johnson, Jamie Shotton, and Julien P. C. Valentin. Fastnerf: High-fidelity neural rendering at 200fps. In *2021 IEEE/CVF International Conference on Computer Vision, ICCV 2021, Montreal, QC, Canada, October 10-17, 2021*, 2021. 3
- [16] Junru Gu, Chenxu Hu, Tianyuan Zhang, Xuanyao Chen, Yilun Wang, Yue Wang, and Hang Zhao. ViP3D: End-to-end visual trajectory prediction via 3d agent queries. In *CVPR, 2023*. 1
- [17] Xingtai Gui, Tengeng Huang, Haonan Shao, Haotian Yao, and Chi Zhang. Fiptr: A simple yet effective transformer framework for future instance prediction in autonomous driving. In *Computer Vision - ECCV 2024 - 18th European Conference, Milan, Italy, September 29-October 4, 2024, Proceedings, Part LXXXVII*, 2024. 1
- [18] Adam W. Harley, Zhaoyuan Fang, Jie Li, Rares Ambrus, and Katerina Fragkiadaki. Simple-BEV: What really matters for multi-sensor bev perception? In *ICRA*, 2023.
- [19] Anthony Hu, Zak Murez, Nikhil Mohan, Sofia Dudas, Jeffrey Hawke, Vijay Badrinarayanan, Roberto Cipolla, and Alex Kendall. FIERY: Future instance segmentation in bird’s-eye view from surround monocular cameras. In *Proceedings of the International Conference on Computer Vision (ICCV)*, 2021. 1
- [20] Shengchao Hu, Li Chen, Penghao Wu, Hongyang Li, Junchi Yan, and Dacheng Tao. ST-P3: end-to-end vision-based autonomous driving via spatial-temporal feature learning. In *Computer Vision - ECCV 2022 - 17th European Conference, Tel Aviv, Israel, October 23-27, 2022, Proceedings, Part XXXVIII*, 2022. 1
- [21] Yihan Hu, Jiazhi Yang, Li Chen, Keyu Li, Chonghao Sima, Xizhou Zhu, Siqi Chai, Senyao Du, Tianwei Lin, Wenhai Wang, Lewei Lu, Xiaosong Jia, Qiang Liu, Jifeng Dai, Yu Qiao, and Hongyang Li. Planning-oriented autonomous driving. In *CVPR, 2023*. 1
- [22] Binbin Huang, Zehao Yu, Anpei Chen, Andreas Geiger, and Shenghua Gao. 2d gaussian splatting for geometrically accurate radiance fields. In *SIGGRAPH 2024 Conference Papers*. Association for Computing Machinery, 2024. 2
- [23] Junjie Huang, Guan Huang, Zheng Zhu, and Dalong Du. Bevdet: High-performance multi-camera 3d object detection in bird-eye-view. *CoRR*, 2021. 6
- [24] Yuanhui Huang, Wenzhao Zheng, Yunpeng Zhang, Jie Zhou, and Jiwen Lu. Tri-perspective view for vision-based 3d semantic occupancy prediction. In *IEEE/CVF Conference on Computer Vision and Pattern Recognition, CVPR 2023, Vancouver, BC, Canada, June 17-24, 2023*, 2023. 1, 2, 6, 7, 8, 3

- [25] Yuanhui Huang, Amonnut Thammatadatrakoon, Wenzhao Zheng, Yunpeng Zhang, Dalong Du, and Jiwen Lu. Gaussianformer-2: Probabilistic gaussian superposition for efficient 3d occupancy prediction. *CoRR*, 2024. 2, 3, 6
- [26] Yuanhui Huang, Wenzhao Zheng, Borui Zhang, Jie Zhou, and Jiwen Lu. Selfocc: Self-supervised vision-based 3d occupancy prediction. In *IEEE/CVF Conference on Computer Vision and Pattern Recognition, CVPR 2024, Seattle, WA, USA, June 16-22, 2024*, pages 19946–19956, 2024. 2, 3, 7
- [27] Yuanhui Huang, Wenzhao Zheng, Yunpeng Zhang, Jie Zhou, and Jiwen Lu. Gaussianformer: Scene as gaussians for vision-based 3d semantic occupancy prediction. In *Computer Vision - ECCV 2024 - 18th European Conference, Milan, Italy, September 29-October 4, 2024, Proceedings, Part XXVII*, 2024. 2, 3, 6
- [28] Haoyi Jiang, Tianheng Cheng, Naiyu Gao, Haoyang Zhang, Tianwei Lin, Wenyu Liu, and Xinggang Wang. Symphonize 3d semantic scene completion with contextual instance queries. In *IEEE/CVF Conference on Computer Vision and Pattern Recognition, CVPR 2024, Seattle, WA, USA, June 16-22, 2024*, 2024. 1, 2, 6, 3
- [29] Xiaohui Jiang, Shuailin Li, Yingfei Liu, Shihao Wang, Fan Jia, Tiancai Wang, Lijin Han, and Xiangyu Zhang. Far3d: Expanding the horizon for surround-view 3d object detection. In *Thirty-Eighth AAAI Conference on Artificial Intelligence, AAAI 2024, Thirty-Sixth Conference on Innovative Applications of Artificial Intelligence, IAAI 2024, Fourteenth Symposium on Educational Advances in Artificial Intelligence, EAAI 2014, February 20-27, 2024, Vancouver, Canada*, 2024. 1
- [30] Kim Jun-Seong, Kim Yu-Ji, Moon Ye-Bin, and Tae-Hyun Oh. Hdr-plenoxels: Self-calibrating high dynamic range radiance fields. In *Computer Vision - ECCV 2022 - 17th European Conference, Tel Aviv, Israel, October 23-27, 2022, Proceedings, Part XXXII*, 2022. 3
- [31] Hiroharu Kato, Yoshitaka Ushiku, and Tatsuya Harada. Neural 3d mesh renderer. In *2018 IEEE Conference on Computer Vision and Pattern Recognition, CVPR 2018, Salt Lake City, UT, USA, June 18-22, 2018*, 2018. 3
- [32] Bernhard Kerbl, Georgios Kopanas, Thomas Leimkühler, and George Drettakis. 3d gaussian splatting for real-time radiance field rendering. *ACM Transactions on Graphics*, 42(4), 2023. 2, 3, 4
- [33] Tarasha Khurana, Peiyun Hu, David Held, and Deva Ramanan. Point cloud forecasting as a proxy for 4d occupancy forecasting. In *IEEE/CVF Conference on Computer Vision and Pattern Recognition, CVPR 2023, Vancouver, BC, Canada, June 17-24, 2023*, 2023. 2
- [34] ByeoungDo Kim, Seong Hyeon Park, Seokhwan Lee, Elbek Khoshimjonov, Dongsuk Kum, Junsoo Kim, Jeong Soo Kim, and Jun Won Choi. Lapred: Lane-aware prediction of multimodal future trajectories of dynamic agents. In *Proceedings of the IEEE/CVF Conference on Computer Vision and Pattern Recognition (CVPR)*, pages 14636–14645, 2021. 1
- [35] Bohan Li, Jiajun Deng, Wenyao Zhang, Zhujin Liang, Dalong Du, Xin Jin, and Wenjun Zeng. Hierarchical temporal context learning for camera-based semantic scene completion. In *Computer Vision - ECCV 2024 - 18th European Conference, Milan, Italy, September 29-October 4, 2024, Proceedings, Part IV*, 2024. 2
- [36] Jinke Li, Xiao He, Chonghua Zhou, Xiaoqiang Cheng, Yang Wen, and Dan Zhang. Viewformer: Exploring spatiotemporal modeling for multi-view 3d occupancy perception via view-guided transformers. In *Computer Vision - ECCV 2024 - 18th European Conference, Milan, Italy, September 29-October 4, 2024, Proceedings, Part XLIII*, 2024. 2
- [37] Yin hao Li, Han Bao, Zheng Ge, Jinrong Yang, Jianjian Sun, and Zeming Li. Bevstereo: Enhancing depth estimation in multi-view 3d object detection with temporal stereo. In *Thirty-Seventh AAAI Conference on Artificial Intelligence, AAAI 2023, Thirty-Fifth Conference on Innovative Applications of Artificial Intelligence, IAAI 2023, Thirteenth Symposium on Educational Advances in Artificial Intelligence, EAAI 2023, Washington, DC, USA, February 7-14, 2023*. 6
- [38] Yin hao Li, Zheng Ge, Guanyi Yu, Jinrong Yang, Zengran Wang, Yukang Shi, Jianjian Sun, and Zeming Li. Bevdepth: Acquisition of reliable depth for multi-view 3d object detection. In *Thirty-Seventh AAAI Conference on Artificial Intelligence, AAAI 2023, Thirty-Fifth Conference on Innovative Applications of Artificial Intelligence, IAAI 2023, Thirteenth Symposium on Educational Advances in Artificial Intelligence, EAAI 2023, Washington, DC, USA, February 7-14, 2023*. 1
- [39] Yiming Li, Zhiding Yu, Christopher B. Choy, Chaowei Xiao, José M. Álvarez, Sanja Fidler, Chen Feng, and Anima Anandkumar. Voxformer: Sparse voxel transformer for camera-based 3d semantic scene completion. In *IEEE/CVF Conference on Computer Vision and Pattern Recognition, CVPR 2023, Vancouver, BC, Canada, June 17-24, 2023*. 1, 6
- [40] Yiming Li, Sihang Li, Xinhao Liu, Moonjun Gong, Kenan Li, Nuo Chen, Zijun Wang, Zhiheng Li, Tao Jiang, Fisher Yu, Yue Wang, Hang Zhao, Zhiding Yu, and Chen Feng. Ssbcbench: A large-scale 3d semantic scene completion benchmark for autonomous driving. In *IEEE/RSJ International Conference on Intelligent Robots and Systems, IROS 2024, Abu Dhabi, United Arab Emirates, October 14-18, 2024*. 5, 6, 1, 2, 3
- [41] Zhiqi Li, Wenhao Wang, Hongyang Li, Enze Xie, Chonghao Sima, Tong Lu, Yu Qiao, and Jifeng Dai. Bevformer: Learning bird’s-eye-view representation from multi-camera images via spatiotemporal transformers. In *Computer Vision - ECCV 2022 - 17th European Conference, Tel Aviv, Israel, October 23-27, 2022, Proceedings, Part IX*, 2022. 1, 6, 3
- [42] Zhiqi Li, Zhiding Yu, David Austin, Mingsheng Fang, Shiyi Lan, Jan Kautz, and José M. Álvarez. FB-OCC: 3d occupancy prediction based on forward-backward view transformation. *CoRR*, 2023. 1
- [43] Yiyi Liao, Jun Xie, and Andreas Geiger. KITTI-360: A novel dataset and benchmarks for urban scene understanding in 2d and 3d. *Pattern Analysis and Machine Intelligence (PAMI)*, 2022. 6, 1
- [44] Xuewu Lin, Tianwei Lin, Zixiang Pei, Lichao Huang, and

- Zhizhong Su. Sparse4d: Multi-view 3d object detection with sparse spatial-temporal fusion. *CoRR*, 2022. 1
- [45] Xuewu Lin, Tianwei Lin, Zixiang Pei, Lichao Huang, and Zhizhong Su. Sparse4d v2: Recurrent temporal fusion with sparse model, 2023.
- [46] Haisong Liu, Yao Teng, Tao Lu, Haiguang Wang, and Limin Wang. Sparsebev: High-performance sparse 3d object detection from multi-camera videos. In *IEEE/CVF International Conference on Computer Vision, ICCV 2023, Paris, France, October 1-6, 2023*. 1
- [47] Hsueh-Ti Derek Liu, Michael Tao, and Alec Jacobson. Paparazzi: surface editing by way of multi-view image processing. *ACM Trans. Graph.*, 37(6):221, 2018. 3
- [48] Lingjie Liu, Jiatao Gu, Kyaw Zaw Lin, Tat-Seng Chua, and Christian Theobalt. Neural sparse voxel fields. In *Advances in Neural Information Processing Systems 33: Annual Conference on Neural Information Processing Systems 2020, NeurIPS 2020, December 6-12, 2020, virtual*, 2020. 3
- [49] Yingfei Liu, Tiancai Wang, Xiangyu Zhang, and Jian Sun. PETR: position embedding transformation for multi-view 3d object detection. In *Computer Vision - ECCV 2022 - 17th European Conference, Tel Aviv, Israel, October 23-27, 2022, Proceedings, Part XXVII*, 2022. 1
- [50] Zhijian Liu, Haotian Tang, Alexander Amini, Xinyu Yang, Huizi Mao, Daniela L. Rus, and Song Han. BEVFusion: Multi-task multi-sensor fusion with unified bird’s-eye view representation. In *ICRA*, 2023. 1
- [51] Yuhang Lu, Xinge Zhu, Tai Wang, and Yuexin Ma. Octreeocc: Efficient and multi-granularity occupancy prediction using octree queries. *CoRR*, 2023. 2
- [52] Qihang Ma, Xin Tan, Yanyun Qu, Lizhuang Ma, Zhizhong Zhang, and Yuan Xie. COTR: compact occupancy transformer for vision-based 3d occupancy prediction. In *IEEE/CVF Conference on Computer Vision and Pattern Recognition, CVPR 2024, Seattle, WA, USA, June 16-22, 2024*, 2024. 2
- [53] Ricardo Martin-Brualla, Noha Radwan, Mehdi S. M. Sajjadi, Jonathan T. Barron, Alexey Dosovitskiy, and Daniel Duckworth. Nerf in the wild: Neural radiance fields for unconstrained photo collections. In *IEEE Conference on Computer Vision and Pattern Recognition, CVPR 2021, virtual, June 19-25, 2021*, 2021. 3
- [54] Ben Mildenhall, Pratul P. Srinivasan, Matthew Tancik, Jonathan T. Barron, Ravi Ramamoorthi, and Ren Ng. Nerf: Representing scenes as neural radiance fields for view synthesis. In *Computer Vision - ECCV 2020 - 16th European Conference, Glasgow, UK, August 23-28, 2020, Proceedings, Part I*, 2020. 2
- [55] Thomas Müller, Alex Evans, Christoph Schied, and Alexander Keller. Instant neural graphics primitives with a multiresolution hash encoding. *arXiv preprint arXiv:2201.05989*, 2022. 2, 3
- [56] Zak Murez, Tarrence van As, James Bartolozzi, Ayan Sinha, Vijay Badrinarayanan, and Andrew Rabinovich. Atlas: End-to-end 3d scene reconstruction from posed images. In *Computer Vision - ECCV 2020 - 16th European Conference, Glasgow, UK, August 23-28, 2020, Proceedings, Part VII*, 2020. 6, 3
- [57] Mingjie Pan, Jiaming Liu, Renrui Zhang, Peixiang Huang, Xiaoqi Li, Hongwei Xie, Bing Wang, Li Liu, and Shanghang Zhang. Renderocc: Vision-centric 3d occupancy prediction with 2d rendering supervision. In *IEEE International Conference on Robotics and Automation (ICRA)*, 2024. 2, 3, 6, 7
- [58] Ri-Zhao Qiu, Ge Yang, Weijia Zeng, and Xiaolong Wang. Language-driven physics-based scene synthesis and editing via feature splatting. In *Computer Vision - ECCV 2024 - 18th European Conference, Milan, Italy, September 29-October 4, 2024, Proceedings, Part XLI*, 2024. 3
- [59] Christian Reiser, Songyou Peng, Yiyi Liao, and Andreas Geiger. Kilonerf: Speeding up neural radiance fields with thousands of tiny mlps. In *2021 IEEE/CVF International Conference on Computer Vision, ICCV 2021, Montreal, QC, Canada, October 10-17, 2021*, 2021. 3
- [60] Jiawei Ren, Liang Pan, Jiaxiang Tang, Chi Zhang, Ang Cao, Gang Zeng, and Ziwei Liu. Dreamgaussian4d: Generative 4d gaussian splatting. *CoRR*, 2023. 3
- [61] Maximilian Schäfer, Kun Zhao, and Anton Kummert. Caspnet++: Joint multi-agent motion prediction. In *IEEE Intelligent Vehicles Symposium, IV 2024, Jeju Island, Republic of Korea, June 2-5, 2024*, 2024. 1
- [62] Yidi Shao, Mu Huang, Chen Change Loy, and Bo Dai. Gausim: Registering elastic objects into digital world by gaussian simulator. *CoRR*, 2024. 3
- [63] Shaoshuai Shi, Li Jiang, Dengxin Dai, and Bernt Schiele. Motion transformer with global intention localization and local movement refinement. *Advances in Neural Information Processing Systems*, 2022. 1
- [64] Shaoshuai Shi, Li Jiang, Dengxin Dai, and Bernt Schiele. Mtr++: Multi-agent motion prediction with symmetric scene modeling and guided intention querying. *arXiv preprint arXiv:2306.17770*, 2023.
- [65] Shaoshuai Shi, Li Jiang, Dengxin Dai, and Bernt Schiele. MTR++: multi-agent motion prediction with symmetric scene modeling and guided intention querying. *IEEE Trans. Pattern Anal. Mach. Intell.*, 2024. 1
- [66] Sathira Silva, Savindu Bhashitha Wannigama, Gihan Jayatilaka, Muhammad Haris Khan, and Roshan Ragel. Unified spatio-temporal tri-perspective view representation for 3d semantic occupancy prediction, 2024. 2
- [67] Carole H Sudre, Wenqi Li, Tom Vercauteren, Sébastien Ourselin, and M. Jorge Cardoso. Generalised dice overlap as a deep learning loss function for highly unbalanced segmentations, 2017. 1
- [68] Qianpu Sun, Changyong Shu, Sifan Zhou, Zichen Yu, Yan Chen, Dawei Yang, and Yuan Chun. Gsrender: Deduplicated occupancy prediction via weakly supervised 3d gaussian splatting. *CoRR*, 2024. 3, 6, 7
- [69] Jiaxiang Tang, Jiawei Ren, Hang Zhou, Ziwei Liu, and Gang Zeng. Dreamgaussian: Generative gaussian splatting for efficient 3d content creation. In *The Twelfth International Conference on Learning Representations, ICLR 2024, Vienna, Austria, May 7-11, 2024*, 2024. 3
- [70] Xiaoyu Tian, Tao Jiang, Longfei Yun, Yucheng Mao, Huitong Yang, Yue Wang, Yilun Wang, and Hang Zhao.

- Occ3d: A large-scale 3d occupancy prediction benchmark for autonomous driving. In *Advances in Neural Information Processing Systems 36: Annual Conference on Neural Information Processing Systems 2023, NeurIPS 2023, New Orleans, LA, USA, December 10 - 16, 2023*, 2023. 5, 6, 7, 8, 1, 2, 3
- [71] Yonglin Tian, Songlin Bai, Zhiyao Luo, Yutong Wang, Yisheng Lv, and Fei-Yue Wang. Mambaocc: Visual state space model for bev-based occupancy prediction with local adaptive reordering. *CoRR*, 2024. 2
- [72] Lening Wang, Wenzhao Zheng, Yilong Ren, Han Jiang, Zhiyong Cui, Haiyang Yu, and Jiwen Lu. Occsora: 4d occupancy generation models as world simulators for autonomous driving. *CoRR*, 2024. 2
- [73] Shihao Wang, Yingfei Liu, Tiancai Wang, Ying Li, and Xiangyu Zhang. Exploring object-centric temporal modeling for efficient multi-view 3d object detection. In *IEEE/CVF International Conference on Computer Vision, ICCV 2023, Paris, France, October 1-6, 2023*, 2023. 1
- [74] Yuxuan Wang, Xuanyu Yi, Zike Wu, Na Zhao, Long Chen, and Hanwang Zhang. View-consistent 3d editing with gaussian splatting. In *Computer Vision - ECCV 2024 - 18th European Conference, Milan, Italy, September 29-October 4, 2024, Proceedings, Part XXXV*, 2024. 3
- [75] Yi Wei, Linqing Zhao, Wenzhao Zheng, Zheng Zhu, Jie Zhou, and Jiwen Lu. Surroundocc: Multi-camera 3d occupancy prediction for autonomous driving. *arXiv preprint arXiv:2303.09551*, 2023. 1, 2, 5, 6, 7, 8, 3
- [76] Christian Witte, Jens Behley, Cyrill Stachniss, and Marvin Raaijmakers. Epipolar attention field transformers for bird's eye view semantic segmentation. *CoRR*, 2024. 1
- [77] Tianyi Xie, Zeshun Zong, Yuxing Qiu, Xuan Li, Yutao Feng, Yin Yang, and Chenfanfu Jiang. Physgaussian: Physics-integrated 3d gaussians for generative dynamics. In *IEEE/CVF Conference on Computer Vision and Pattern Recognition, CVPR 2024, Seattle, WA, USA, June 16-22, 2024*, 2024. 3
- [78] Haolin Xiong, Sairisheek Muttukuru, Rishi Upadhyay, Pradyumna Chari, and Achuta Kadambi. Sparsegts: Real-time 360° sparse view synthesis using gaussian splatting. *Arxiv*, 2023. 2
- [79] Chenyu Yang, Yuntao Chen, Hao Tian, Chenxin Tao, Xizhou Zhu, Zhaoxiang Zhang, Gao Huang, Hongyang Li, Yu Qiao, Lewei Lu, Jie Zhou, and Jifeng Dai. Bevformer v2: Adapting modern image backbones to bird's-eye-view recognition via perspective supervision. In *IEEE/CVF Conference on Computer Vision and Pattern Recognition, CVPR 2023, Vancouver, BC, Canada, June 17-24, 2023*, 2023. 1
- [80] Yu Yang, Jianbiao Mei, Yukai Ma, Siliang Du, Wenqing Chen, Yijie Qian, Yuxiang Feng, and Yong Liu. Driving in the occupancy world: Vision-centric 4d occupancy forecasting and planning via world models for autonomous driving. *CoRR*, 2024. 2
- [81] Zetong Yang, Li Chen, Yanan Sun, and Hongyang Li. Visual point cloud forecasting enables scalable autonomous driving. In *Proceedings of the IEEE/CVF Conference on Computer Vision and Pattern Recognition*, 2024. 1
- [82] Mingqiao Ye, Martin Danelljan, Fisher Yu, and Lei Ke. Gaussian grouping: Segment and edit anything in 3d scenes. In *Computer Vision - ECCV 2024 - 18th European Conference, Milan, Italy, September 29-October 4, 2024, Proceedings, Part XXIX*, 2024. 3
- [83] Tengju* Ye, Wei* Jing, Chunyong Hu, Shikun Huang, Linqing Gao, Fangzhen Li, Jingke Wang, Ke Guo, Wencong Xiao, Weibo Mao, Hang Zheng, Kun Li, Junbo Chen, and Kaicheng Yu. Fusionad: Multi-modality fusion for prediction and planning tasks of autonomous driving. *arXiv preprint arXiv:2308.01006*, 2023. *Equal Contribution. 1
- [84] Zhangchen Ye, Tao Jiang, Chenfeng Xu, Yiming Li, and Hang Zhao. Cvt-occ: Cost volume temporal fusion for 3d occupancy prediction. In *Computer Vision - ECCV 2024 - 18th European Conference, Milan, Italy, September 29-October 4, 2024, Proceedings, Part LXXXIII*, 2024. 2
- [85] Taoran Yi, Jiemin Fang, Junjie Wang, Guanjun Wu, Lingxi Xie, Xiaopeng Zhang, Wenyu Liu, Qi Tian, and Xinggang Wang. Gaussiandreamer: Fast generation from text to 3d gaussians by bridging 2d and 3d diffusion models. In *IEEE/CVF Conference on Computer Vision and Pattern Recognition, CVPR 2024, Seattle, WA, USA, June 16-22, 2024*, 2024. 3
- [86] Alex Yu, Ruilong Li, Matthew Tancik, Hao Li, Ren Ng, and Angjoo Kanazawa. Plenotrees for real-time rendering of neural radiance fields. In *2021 IEEE/CVF International Conference on Computer Vision, ICCV 2021, Montreal, QC, Canada, October 10-17, 2021*, 2021. 3
- [87] Zehao Yu, Anpei Chen, Binbin Huang, Torsten Sattler, and Andreas Geiger. Mip-splatting: Alias-free 3d gaussian splatting. *Conference on Computer Vision and Pattern Recognition (CVPR)*, 2024. 2
- [88] Ye Yuan, Xinshuo Weng, Yanglan Ou, and Kris Kitani. Agentformer: Agent-aware transformers for socio-temporal multi-agent forecasting. In *Proceedings of the IEEE/CVF International Conference on Computer Vision (ICCV)*, 2021. 1
- [89] Dongbin Zhang, Chuming Wang, Weitao Wang, Peihao Li, Minghan Qin, and Haoqian Wang. Gaussian in the wild: 3d gaussian splatting for unconstrained image collections. *arXiv preprint arXiv:2403.15704*, 2024. 2
- [90] Yunpeng Zhang, Zheng Zhu, Wenzhao Zheng, Junjie Huang, Guan Huang, Jie Zhou, and Jiwen Lu. BEVerse: Unified perception and prediction in birds-eye-view for vision-centric autonomous driving. *arXiv preprint arXiv:2205.09743*, 2022. 1
- [91] Yunpeng Zhang, Zheng Zhu, and Dalong Du. Occformer: Dual-path transformer for vision-based 3d semantic occupancy prediction. In *IEEE/CVF International Conference on Computer Vision, ICCV 2023, Paris, France, October 1-6, 2023*, 2023. 6, 3
- [92] Linqing Zhao, Xiuwei Xu, Ziwei Wang, Yunpeng Zhang, Borui Zhang, Wenzhao Zheng, Dalong Du, Jie Zhou, and Jiwen Lu. Lowrankocc: Tensor decomposition and low-rank recovery for vision-based 3d semantic occupancy prediction. In *IEEE/CVF Conference on Computer Vision and Pattern Recognition, CVPR 2024, Seattle, WA, USA, June 16-22, 2024*, 2024. 2

- [93] Wenzhao Zheng, Junjie Wu, Yao Zheng, Sicheng Zuo, Zixun Xie, Longchao Yang, Yong Pan, Zhihui Hao, Peng Jia, Xianpeng Lang, and Shanghang Zhang. Gaussianad: Gaussian-centric end-to-end autonomous driving. *CoRR*, 2024. 3
- [94] Brady Zhou and Philipp Krähenbühl. Cross-view transformers for real-time map-view semantic segmentation. In *IEEE/CVF Conference on Computer Vision and Pattern Recognition, CVPR 2022, New Orleans, LA, USA, June 18-24, 2022*, 2022. 1
- [95] Zhuofan Zong, Dongzhi Jiang, Guanglei Song, Zeyue Xue, Jingyong Su, Hongsheng Li, and Yu Liu. Temporal enhanced training of multi-view 3d object detector via historical object prediction. In *IEEE/CVF International Conference on Computer Vision, ICCV 2023, Paris, France, October 1-6, 2023*, 2023. 1
- [96] Jian Zou, Tianyu Huang, Guanglei Yang, Zhenhua Guo, Tao Luo, Chun-Mei Feng, and Wangmeng Zuo. Unim²ae: Multi-modal masked autoencoders with unified 3d representation for 3d perception in autonomous driving. In *Computer Vision - ECCV 2024 - 18th European Conference, Milan, Italy, September 29-October 4, 2024, Proceedings, Part XXII*, 2024. 1
- [97] Sicheng Zuo, Wenzhao Zheng, Yuanhui Huang, Jie Zhou, and Jiwen Lu. Gaussianworld: Gaussian world model for streaming 3d occupancy prediction. *CoRR*, 2024. 3

GaussRender: Learning 3D Occupancy with Gaussian Rendering

Supplementary Material

A. Datasets

The evaluation is performed on three datasets: SurroundOcc-nuScenes [75], Occ3d-nuScenes [70], and SSCBench-Kitti360 [40].

SurroundOcc-nuScenes and Occ3D-nuScenes are derived from the nuScenes dataset [5]. nuScenes provides 1000 scenes of surround view driving scenes in Boston and Singapore split in three sets train/val/test of size 700/150/150 scenes. Each comprises 20 seconds long and is fully annotated at 2Hz using one ground truth from 5 radars, 6 cameras at resolution 900×1600 pixels, one LiDAR, and one IMU. From the LiDAR annotations, SurroundOcc-nuScenes [75] derived a 3D grid of shape $[200, 200, 16]$ with a range in $[-50, 50] \times [-50, 50] \times [-5, 3]$ meters at a spatial resolution of $[0.5, 0.5, 0.5]$ meters, annotated with 17 different classes, 1 representing empty and 16 for the semantics. The Occ3d-nuScenes [70] dataset has a lower voxel size of 0.4 meters in all directions while keeping the same voxel grid shape with a range of $[-40, 40] \times [-40, 40] \times [-1, 5.4]$ meters. It contains 18 classes: 1 representing empty, 16 for the semantics, and 1 for others.

SSCBench-Kitti360 [40] is derived from the Kitti360 dataset [43]. Kitti360 consists of over 320k images shot by 2 front cameras at a resolution 1408×376 pixels and two fisheye cameras in the suburban area covering a driving distance of 73.7km. Only one camera is used in the 3D occupancy task. SSCBench-Kitti360 [40] annotates for each sequence a voxel grid of shape $[256, 256, 32]$ with a range in $[0, 51.2] \times [-25.6, 25.6] \times [-2, 4.4]$ meters at a voxel resolution of 0.2 in all directions. The provided voxel grid is annotated with 19 classes: 1 representing empty and 18 the semantics.

B. Models and implementation details

We integrate our rendering module and associated loss into three different models: **SurroundOcc** [75] (multi-scale voxel-based approach), **TPVFormer** [24] (triplane-based approach), and **Symphonies** [28] (voxel-with-instance query-based approach). Each model is retrained using the same training settings, following the optimization parameters from SurroundOcc. No extensive hyperparameter searches are conducted on the learning rate; the goal is to demonstrate that the loss can be integrated at minimal cost into existing pipelines. All models were trained for 20 epochs on 4 A100 or H100 GPUs with a batch size of

Data	Model	Tr. time (HH:MM)	Memory usage (GB)
Sur.Occ-nusc	TPVFormer	21:44	25.3GB
	+GaussRender	24:00 +10.4%	28.1GB +11.1%
	SurroundOcc	26:38	23.0GB
	+GaussRender	29:19 +10.5%	24.2GB +5.2%
SSCB.K.360	TPVFormer	7:02	29.3GB
	+GaussRender	8:16 +14.0%	31.7GB +8.2%
	SurroundOcc	11:12	15.5GB
	+GaussRender	11:56 +6.1%	17.6GB +13.5%

Table 5. **Training Time and GPU Memory Usage** across models and datasets without or with our module using four renderings per scene, two for BeV (ground truth and predictions) and two for another camera (ground truth and predictions). Test performed on a 40GB A100.

1, using an AdamW optimizer with a learning rate of $2e^{-4}$ and a weight decay of 0.01. For each combination of models and datasets, we evaluated existing checkpoints if provided; otherwise, we reported the scores from previous papers when available, or we re-trained the models. In particular, we retrained SurroundOcc on Occ3D-nuScenes and SSCBench-KITTI360 and we used the official checkpoint for Symphonies [28] while noticing there is a discrepancy in IoU / mIoU between the reported value in the paper and the actual one of the official checkpoint, as explained in their GitHub issue ¹.

C. Computational cost

Our module introduces a memory overhead for each rendering it performs. If we want to select cameras dynamically during training, we will therefore run each rendering for predictions and annotations. As our rendering strategy selects a camera and always keeps the BeV, we therefore have 2 renderings per input, making a total of 4 renderings at each iteration. As illustrated in the table, the additional cost in terms of memory and time is low Tab. 5 even if in the two datasets studied, the renderings are in very high resolution. In addition, if we pre-select camera locations, we can pre-process the annotation renderings, and we can always render at a lower resolution if needed.

D. Gaussian scaling

In addition to the quantitative justification presented in the paper, we can see qualitatively in Fig. 7 the impact of the

¹<https://github.com/hustvl/Symphonies/issues/5>

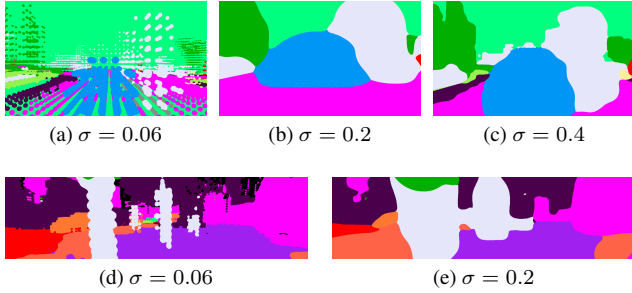


Figure 8. **Visualization of different Gaussianized Voxels for different Datasets and Scales.** The first row represents data from Occ3d-nuScenes [70] while the second and third rows are data from SSCBench-Kitti360 [40].

scale on the rendering. We need to find the right balance: if the Gaussians are too large, only a few will cover the entire image and the loss will be backpropagated mainly from the closest elements. Conversely, if the Gaussians are too small, gaps will appear between the voxels, resulting in a sparse activation that causes the model to render only the empty class, yielding very low metric values.

E. Scores detailed per class

The following tables give the detailed IoU and mIoU scores of the models studied for each dataset. [Tab. 7](#) concerns the Occ3D-nuScenes dataset [70], [Tab. 8](#) the SSCBench-KITTI360 dataset [40] and [Tab. 6](#) the SurroundOcc-nuScenes dataset [75].

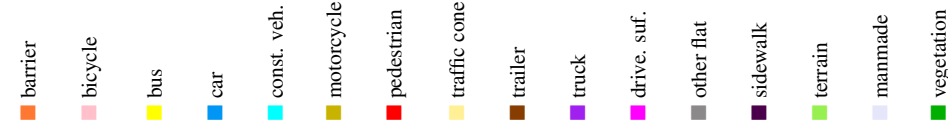
Model																			
	IoU	mIoU	barrier	bicycle	bus	car	const. veh.	motorcycle	pedestrian	traffic cone	trailer	truck	drive. suf.	other flat	sidewalk	terrain	manmade	vegetation	
MonoScene [6]	23.96	7.31	4.03	0.35	8.00	8.04	2.90	0.28	1.16	0.67	4.01	4.35	27.72	5.20	15.13	11.29	9.03	14.86	
Atlas [56]	28.66	15.00	10.64	5.68	19.66	24.94	8.90	8.84	6.47	3.28	10.42	16.21	34.86	15.46	21.89	20.95	11.21	20.54	
BEVFormer [41]	30.50	16.75	14.22	6.58	23.46	28.28	8.66	10.77	6.64	4.05	11.20	17.78	37.28	18.00	22.88	22.17	13.80	22.21	
TPVFormer-lidar [24]	11.51	11.66	16.14	7.17	22.63	17.13	8.83	11.39	10.46	8.23	9.43	17.02	8.07	13.64	13.85	10.34	4.90	7.37	
OccFormer [91]	31.39	19.03	18.65	10.41	23.92	30.29	10.31	14.19	13.59	10.13	12.49	20.77	38.78	19.79	24.19	22.21	13.48	21.35	
GaussianFormer [27]	29.83	19.10	19.52	11.26	26.11	29.78	10.47	13.83	12.58	8.67	12.74	21.57	39.63	23.28	24.46	22.99	9.59	19.12	
GaussianFormerv2 [25]	30.56	20.02	20.15	12.99	27.61	30.23	11.19	15.31	12.64	9.63	13.31	22.26	39.68	23.47	25.62	23.20	12.25	20.73	
TPVFormer [24]	30.86	17.10	15.96	5.31	23.86	27.32	9.79	8.74	7.09	5.20	10.97	19.22	38.87	21.25	24.26	23.15	11.73	20.81	
w/ GaussRender	32.05	20.85	20.2	13.06	28.95	30.96	11.26	16.69	13.64	10.57	12.77	22.58	40.69	23.49	26.41	24.97	14.41	22.94	
(gain)	1.19	3.75	4.24	7.75	5.09	3.64	1.47	7.95	6.55	5.37	1.80	3.36	1.82	2.24	2.15	1.82	2.68	2.13	
SurroundOcc [75]	31.49	20.30	20.59	11.68	28.06	30.86	10.70	15.14	14.09	12.06	14.38	22.26	37.29	23.70	24.49	22.77	14.89	21.86	
w/ GaussRender	32.61	20.82	20.32	13.22	28.32	31.05	10.92	15.65	12.84	8.91	13.29	22.76	41.22	24.48	26.38	25.20	15.31	23.25	
(gain)	1.12	0.52	-0.27	1.54	0.26	0.19	0.22	0.51	-1.25	-3.15	-1.09	0.50	3.93	0.78	1.89	2.43	0.42	1.39	

Table 6. **Semantic voxel occupancy results on the SurroundOcc-NuScenes [75] validation set.** The best results are in bold. Our module GaussRender achieves state-of-the-art performance when integrated with standard models. Previous results are reported from [25].

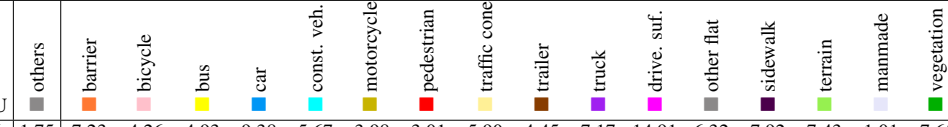
Method	Input																			
		mIoU	others	barrier	bicycle	bus	car	const. veh.	motorcycle	pedestrian	traffic cone	trailer	truck	drive. suf.	other flat	sidewalk	terrain	manmade	vegetation	
MonoScene	Voxels	6.06	1.75	7.23	4.26	4.93	9.38	5.67	3.98	3.01	5.90	4.45	7.17	14.91	6.32	7.92	7.43	1.01	7.65	
BEVDet	Voxels	19.38	4.39	30.31	0.23	32.26	34.47	12.97	10.34	10.36	6.26	8.93	23.65	52.27	24.61	26.06	22.31	15.04	15.10	
OccFormer	Voxels	21.93	5.94	30.29	12.32	34.40	39.17	14.44	16.45	17.22	9.27	13.90	26.36	50.99	30.96	34.66	22.73	6.76	6.97	
BEVStereo	Voxels	24.51	5.73	38.41	7.88	38.70	41.20	17.56	17.33	14.69	10.31	16.84	29.62	54.08	28.92	32.68	26.54	18.74	17.49	
BEVFormer	Voxels	26.88	5.85	37.83	17.87	40.44	42.43	7.36	23.88	21.81	20.98	22.38	30.70	55.35	28.36	36.0	28.06	20.04	17.69	
CTF-Occ	Voxels	28.53	8.09	39.33	20.56	38.29	42.24	16.93	24.52	22.72	21.05	22.98	31.11	53.33	33.84	37.98	33.23	20.79	18.0	
RenderOcc	Lidar	23.93	5.69	27.56	14.36	19.91	20.56	11.96	12.42	12.14	14.34	20.81	18.94	68.85	33.35	42.01	43.94	17.36	22.61	
RenderOcc	Voxels+Lidar	26.11	4.84	31.72	10.72	27.67	26.45	13.87	18.2	17.67	17.84	21.19	23.25	63.2	36.42	46.21	44.26	19.58	20.72	
TPVFormer	Voxels	27.83	7.22	38.90	13.67	40.78	45.90	17.23	19.99	18.85	14.30	26.69	34.17	55.65	35.47	37.55	30.70	19.40	16.78	
TPVFormer w. GR	Voxels	30.48	9.84	42.3	24.09	41.79	46.49	18.22	25.85	25.06	22.53	22.9	33.34	58.86	33.19	36.57	31.84	23.55	21.8	
(gain)		2.65	2.62	3.40	10.42	1.01	0.59	0.99	5.86	6.21	8.23	-3.79	-0.83	3.21	-2.28	-0.98	1.14	4.15	5.02	
SurroundOcc	Voxels	29.21	8.64	40.12	23.36	39.89	45.23	17.99	24.91	22.66	18.11	21.64	32.5	57.6	34.1	35.68	32.54	21.27	20.27	
SurroundOcc w. GR	Voxels	30.38	8.87	40.98	23.25	43.76	46.37	19.49	25.2	23.96	19.08	25.56	33.65	58.37	33.28	36.41	33.21	22.76	22.19	
(gain)		1.17	0.23	0.86	-0.11	3.87	1.14	1.50	0.29	1.30	0.97	3.92	1.15	0.77	-0.82	0.73	0.67	1.49	1.92	

Table 7. **Semantic voxel occupancy results on the Occ3D-nuScenes [70] validation set.** The best results are in bold. Our module GaussRender achieves state-of-the-art performance when integrated with standard models. Previous results are reported from [25, 57].

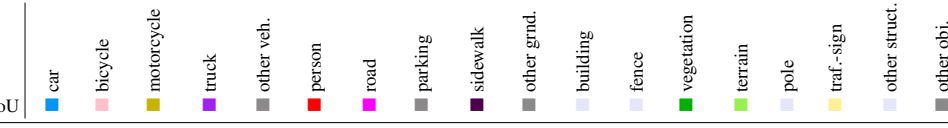
Method																					
	IoU	mIoU	car	bicycle	motorcycle	truck	other veh.	person	road	parking	sidewalk	other gmd.	building	fence	vegetation	terrain	pole	traf.-sign	other struct.	other obj.	
MonoScene *	37.87	12.31	19.34	0.43	0.58	8.02	2.03	0.86	48.35	11.38	28.13	3.32	32.89	3.53	26.15	16.75	6.92	5.67	4.20	3.09	
VoxFormer *	38.76	11.91	17.84	1.16	0.89	4.56	2.06	1.63	47.01	9.67	27.21	2.89	31.18	4.97	28.99	14.69	6.51	6.92	3.79	2.43	
OccFormer *	40.27	13.81	22.58	0.66	0.26	9.89	3.82	2.77	54.30	13.44	31.53	3.55	36.42	4.80	31.00	19.51	7.77	8.51	6.95	4.60	
SurroundOcc	38.51	13.08	21.31	0.0	0.0	6.05	4.29	0.0	53.88	12.56	30.89	2.57	34.93	3.59	29.03	16.98	5.61	6.66	4.39	2.62	
SurroundOcc w. GR	38.62	13.34	21.61	0.0	0.0	6.75	4.5	0.0	53.64	11.93	30.24	2.67	35.01	4.55	29.81	17.32	6.19	8.49	4.8	2.59	
(gain)	0.11	0.26	0.30	0.0	0.0	0.70	0.21	0.0	-0.24	-0.63	-0.65	0.10	0.08	0.96	0.78	0.34	0.58	1.83	0.41	-0.03	
Symphonies (official checkpoint)	43.40	17.82	26.86	4.21	4.92	14.19	7.67	16.79	57.31	13.60	35.25	4.58	39.20	7.96	34.23	19.20	8.22	16.79	6.03	6.03	
Symphonies w. GR	44.08	18.11	27.37	3.24	5.12	14.69	8.76	16.70	58.05	13.87	35.70	4.76	40.09	7.88	34.76	19.20	8.22	16.49	8.64	6.50	
(gain)	+0.68	+0.29	+0.51	-0.97	+0.20	+0.50	+1.09	-0.09	+0.74	+0.27	+0.45	+0.18	+0.89	-0.08	+0.53	0.00	0.00	-0.30	+2.61	+0.47	

Table 8. **Semantic voxel occupancy results on the SSCBench-KITTI360 [40] test set.** The best results are in bold. Our module GaussRender achieves state-of-the-art performance when integrated with standard models. Previous results are reported from [28].